Atmos. Chem. Phys. Discuss., 13, 25253–25290, 2013
www.atmos-chem-phys-discuss.net/13/25253/2013/
doi:10.5194/acpd-13-25253-2013

Atmospheric Chemistry and Physics Discussions

Factors controlling pollutant plume length downwind of major roadways in nocturnal surface inversions

W. Choi[1], **A. M. Winer**[2], **and S. E. Paulson**[1]

[1]University of California, Los Angeles, Department of Atmospheric and Oceanic Sciences, Los Angeles, California, USA
[2]University of California, Los Angeles, School of Public Health, Environmental Health Sciences Department, Los Angeles, California, USA

Received: 19 April 2013 – Accepted: 11 September 2013 – Published: 30 September 2013

Correspondence to: S. E. Paulson (paulson@atmos.ucla.edu)

Published by Copernicus Publications on behalf of the European Geosciences Union.

Abstract

A curve fit method using a Gaussian dispersion model solution was successfully applied to obtain both dispersion coefficients and a particle number emission factor (PNEF) directly from ultrafine particle (UFP) concentration profiles observed downwind of major roadways in California's South Coast Air Basin (SoCAB). The Briggs' formulation for the vertical dispersion parameter σ_z was adopted in this study due to its better performance in describing the observed profiles compared to other formulations examined. The two dispersion coefficients in Briggs' formulation, α and β, ranged from 0.02 to 0.07 and from -0.5×10^{-3} to 2.8×10^{-3}, respectively, for the four freeway transects studied and are significantly different for freeways passing over vs. under the street on which measurements of the freeway plume were made. These ranges are wider than literature values for α and β under stable conditions. The dispersion coefficients derived from observations showed strong correlations with both surface meteorology (wind speed/direction, temperature, and air stability) and differences in concentrations between the background and plume peak. The relationships were applied to predict freeway plume transport using a multivariate regression, and produced excellent agreement with observed UFP concentration profiles. The mean PNEF for a mixed vehicle fleet on the four freeways was estimated as 1.2×10^{14} particles mi^{-1} $\mathrm{vehicle}^{-1}$, which is about 15 % of the value estimated in 2001 for the I-405 freeway, implying significant reductions in UFP emissions over the past decade in the SoCAB.

1 Introduction

Numerous epidemiological and toxicological studies have shown that ultrafine particles (UFP) cause various adverse health effects, such as respiratory illness, DNA damage, cardiovascular disease, and adverse birth outcomes (Hoek et al., 2010; Knol et al., 2009; Moller et al., 2008). The dominant source of UFP in urban areas is vehicular emissions (Pey et al., 2009). UFP account for the major proportion (~ 80 %) of total

ACPD
13, 25253–25290, 2013

particulate matter (PM) number concentration but a negligible proportion of the mass concentration (Kumar et al., 2010). PM mass ($PM_{2.5}$ and PM_{10}) is currently regulated but PM numbers are not, thus measurements of ambient UFP are relatively sparse.

Although a number of studies on UFP emissions from major roadways and their spatial impacts have recently been conducted, the sampling conditions in most studies were limited to the daytime unstable convective boundary layer (Karner et al., 2010). However, Hu et al. (2009) found a wide UFP impact area up to 2 km downwind of the I-10 freeway during stable pre-sunrise hours in Santa Monica, California. Subsequently, Choi et al. (2012) extended this result, reporting the prevalence of wide area impacts (1500 m to more than 2500 m) downwind of freeways under stable pre-sunrise conditions at several additional locations throughout the South Coast Air Basin (SoCAB). Choi et al. (2012) also found the decay constant of UFP concentrations with distance under stable conditions is about an order of magnitude smaller than that during daytime.

Although the dominant factor causing differences in dispersion/dilution rates between nocturnal (or stable) and daytime (or well mixed) conditions is clearly atmospheric stability combined with different boundary layer heights (Kerminen et al., 2007; Hu et al., 2009; Hussein et al., 2006; Zhu et al., 2006), quantitative and systematic meteorological dependencies of the decay of primary pollutants with distance downwind of major roads have yet to be developed, particularly for stable atmospheres. This gap prevents the reliable prediction of the extent and magnitude of roadway plumes under stable conditions when their larger downwind extent potentially impacts large populations.

Many studies have attempted to predict the pollutant concentrations from vehicular emissions near roadways using various dispersion models (Sharma and Khare, 2001). However, most studies have focused on predicting elevated pollutant concentrations at specific distances from sources rather than describing concentration profiles. A few studies attempted to reproduce UFP concentration profiles obtained at multiple discrete distances within short ranges (< 300 m) during daytime conditions (Zhu and Hinds, 2005; Gramotnev et al., 2003).

ACPD
13, 25253–25290, 2013

Gaussian dispersion models have been commonly used to explain spatial concentration variations from line sources (e.g., Sharma and Khare, 2001; Chen et al., 2009; Briant et al., 2011; Gramotnev et al., 2003; Kumar et al., 2011). In this model, parameterization of dispersion coefficients is critical to calculate pollutant concentrations at specific distances from the source. Existing parameterizations of the dispersion coefficients are based on Pasquill stability classes (Pasquill, 1961). However, the Pasquill parameterization has only two classes for stable conditions (Table 1), and thus has limited ability to explain the variations in concentration profiles under stable conditions.

In the present study, the effectiveness of the Gaussian dispersion model solution to fit observed UFP concentration profiles is examined, and both dispersion coefficients and emission factors are obtained directly from the observations. In addition, the quantitative effects of meteorological parameters and the role of background-subtracted plume concentrations on plume extensions are investigated. Appropriate parameterization of dispersion coefficients and emission factors based on observable variables can provide predictive capability for the extent of freeway plumes under stable conditions.

2 Methods

2.1 Sampling areas and transects

The analyses are carried out for the detailed dataset collected by Choi et al. (2012) with a mobile measurement platform (MMP) in the early morning before sunrise at four locations in the SoCAB. The downtown Los Angeles (DTLA), Paramount, Carson, and Claremont transects traveled along N. Coronado St., Obispo St., 228th St., and N. Mountain Ave., respectively, and crossed perpendicular to the respective freeways, the 101, 91, I-110, and I-210 freeways. All transects were small two lane streets through residential areas. For the DTLA and Paramount transects, the 101 and 91 freeways passed over the measurement routes, and for the Carson and Claremont transects, the I-110 and I-210 freeways passed under the routes. The DTLA transect was located

ACPD
13, 25253–25290, 2013

~22 km from the ocean, and the Paramount and Carson transects were located about 8–10 km from the ocean, whereas the Claremont transect was located further inland (~50 km east from DTLA and ~70 km from the coast), at the foot of the steeply rising San Gabriel Mountains. More details about transects and surroundings are provided in Choi et al. (2012).

2.2 Instrumentation, sampling, and data analysis

A pollution-free Toyota RAV4 sub-SUV electric vehicle served as the MMP in the present study. UFP measurements were conducted with 1 s time resolution using a fast mobility particle sizer (FMPS) and condensation particle counter (CPC). Measurements of nitric oxide, carbon monoxide, particle-bound polycyclic aromatic hydrocarbon, $PM_{2.5}$, PM_{10}, and black carbon, were also conducted. Instruments and calibrations are described in detail elsewhere (Choi et al., 2012; Hu et al., 2009; Kozawa et al., 2009; Westerdahl et al., 2005). Here we focus on UFP concentration profiles during the stable pre-sunrise hours in the SoCAB. UFP provide the clearest profiles, due to a combination of fast response instrumentation and a greater dynamic range of pollutant concentrations. The latter results from a low background level, due to the relatively short UFP lifetime (Capaldo and Pandis, 2001).

Measurements were conducted during the pre-sunrise hours (04:30–06:30 LT) in the winter to spring seasons for the DTLA, Paramount, and Carson transects (January to March), and in Claremont during May and June of 2011 (Table 2). The MMP was driven at roughly constant slow speeds (below 20 mph) during sampling whenever possible (allowing for stop signs and traffic lights). Data were logged every second in a Eurotherm Chessell Graphic DAQ Recorder. In order to synchronize the instrumental response times, a time-lag correlation method was used (Choi et al., 2012). Local impacts of individual high-emission vehicles encountered on a transect were removed by a running low 25 % quantile method (Choi et al., 2012). Any remaining local effects were examined and removed by reviewing video and audio records to verify proximity of a high emitting vehicle.

ACPD
13, 25253–25290, 2013

Averaged surface meteorology (temperature, wind speed and direction, and relative humidity) was obtained with 2-D sonic anemometer and temperature/humidity sensors located on the roof the MMP, for about 5 min. just prior to and following every transect run. Vertical gradients of temperature, humidity, and wind speed/direction were obtained once per day with a balloon tethersonde (SmartTether™, Anasphere Inc.) before the measurements at locations within 1–5 km of the transects. Closer proximity was not possible because of the high density of airports and airstrips (regulations prohibit tethered balloon flights within 5 mi of an airport) and urban development, which provides few unobstructed areas for balloon-borne measurements.

Traffic flow data were collected for the four freeways from the Freeway Performance Measurement System (PeMS) operated by the Institute of Transportation at University of California, Berkeley. The locations of traffic flow sensors and other details concerning instrumentation, measurements and data analysis are available in Choi et al. (2012).

2.3 Theory and curve fits

2.3.1 Development of a curve fit equation

A Gaussian dispersion model solution assuming an infinite line source was applied as a basic equation for curve fits to the observed concentration profiles (Eq. 1):

$$C(x,z) = \frac{Q}{\sqrt{2\pi}\sigma_z(x)\cdot U_e}\left[\exp\left(-\frac{(z+H)^2}{2\sigma_z^2(x)}\right)+\exp\left(-\frac{(z-H)^2}{2\sigma_z^2(x)}\right)\right] \quad (1)$$

where Q is an emission rate, U_e is an effective wind speed (ambient wind + speed correction due to traffic wake), z is height, H is the height of the emission source, and σ_z is the standard deviation of the time-averaged concentration distributions in the vertical direction at distance x from the source (Luhar and Patil, 1989). An infinite line source assumption is reasonable for the present study due to the long length of freeways (more than 20 km) compared to relatively short downwind length scale of transects (~ 2 km).

ACPD
13, 25253–25290, 2013

Equation (1) is simplified to obtain a final curve fit equation (Eq. 2), where Q_c represents a bulk emission parameter including emission rate (Q) combined with wind effects (U_e), and remains as a free variable to be determined from observed concentration profiles.

$$C(x,z) = \frac{Q_c}{\sigma_z}\left[\exp\left(-\frac{(z+H)^2}{2\sigma_z^2}\right) + \exp\left(-\frac{(z-H)^2}{2\sigma_z^2}\right)\right] \quad (2)$$

The final step to formulate a curve fit equation is to parameterize σ_z. For this, two common methods were examined: Chock's (1978) and Briggs' (1973) formulas, which were used by Luhar and Patil (1989) and Briant et al. (2011), respectively, in their model evaluations. However, we note that both Chock's and Briggs' formulas have just one or two equations for stable atmospheres, based on land use (e.g., urban and rural). Thus, neither formula is sufficient to explain the meteorology-dependent variations in observed freeway plume decay during stable pre-sunrise hours. To account for these limits, two coefficients in Chock's and Briggs' formulas were held as free variables in the curve fit equation (e.g., α and β for Briggs formula in Eq. 3). We found that the Briggs' formula form more successfully described the observed concentration profiles. The Briggs expression has slightly different formulations for rural and urban conditions (Table 1), the choice of which affects one of the two dispersion coefficients (β). Both forms fit the data equally well and produce nearly identical curve shapes. For three of our four transects the dispersion coefficients returned by the formulation β is more consistent with the rural form (described more below). While this may seem surprising, much of Los Angeles, including these three transects, consist of single story residential development. The fourth transect, DTLA, has tall buildings in the area (although few are on the transect itself), and its β values are closer to expected urban values. Here, we use the rural form of the Briggs' formula as the basic equation for fitting the observations, to allow us to investigate meteorological and traffic effects on plume intensities and transport among the different sites. More discussion of the observed α and β are presented in

ACPD
13, 25253–25290, 2013

Sect. 3.1.

$$\sigma_z(x) = \frac{\alpha \cdot x}{1 + \beta \cdot x} \quad (3)$$

Curve fit results using Chock's formula tended to underestimate the peak concentrations near freeways. Additionally, we examined a K-theory model developed by Sharan and Yadav (1998) for dispersion of pollutants from a point source under stable conditions with light winds (Table 1). Zhu and Hinds (2005) modified the K-theory model for a line source to explain the decay of a freeway plume during daytime. The curve fits with the K-theory model yielded poorer fits to our nocturnal observations in the far downwind areas compared to the Gaussian model with the Briggs formulation for σ_z above. Consequently, Eq. (2) combined with Eq. (3) was used to fit the observed data using the least squares method.

Although particle number concentrations are influenced by particle dynamics such as coagulation, deposition, and condensation/evaporation, a common conclusion from previous studies is that dilution is the most important process controlling particle number (e.g., Kumar et al., 2011). Particularly near emission sources, such as the curbside of a major road, the dilution timescale is approximately one to two orders of magnitude faster than deposition and coagulation, respectively (Kumar et al., 2011). Even under stable nocturnal conditions, dilution appears to be the most important sink accounting for ~70 % of the overall decay rates (Choi and Paulson, 2013). Because here we extract dispersion parameters (α and β) by fitting the observed UFP profiles, α and β include particle dynamics effects together with dispersion/dilution effects on observed plume decay rates.

2.3.2 Curve fit parameters (Q_c, α, and β)

The emission parameter Q_c, which represents the wind speed-corrected emission factor, influences only the magnitude of the peak and the overall pollutant concentrations. Thus, this method allows us to estimate an emission factor for a mixed vehicle fleet

ACPD
13, 25253–25290, 2013

on major roads directly from the observed concentration profiles. The details of this analysis are discussed in Sect. 3.5.

Pollutant profiles simulated with Eqs. (2) and (3) clearly show that as α decreases, holding β constant, the freeway plume peak appears farther downwind of the emission source with elevated downwind concentrations, allowing pollutants to be transported farther downwind (Fig. 1a). With fixed α, decreasing β results in more rapid dissipation of the plume, but the peak location is unaffected (Fig. 1b).

Here, we explore the values for α and β derived by fitting Eqs. (2) and (3) to the daily measurement period average data, in order to quantitatively investigate the effects of both meteorology and traffic density on the magnitude of peak concentrations and decay rates of freeway plumes (Table 2). If α and β can be properly parameterized with measurable properties such as surface meteorology, it will be possible to predict how widely freeway plumes influence vehicle-related pollutant concentrations in neighborhoods downwind of freeways under stable atmospheric conditions.

Peak concentrations can be directly influenced by vehicle number and type (and other characteristics), passing on the freeway at the moment when the MMP crosses under or over the freeway, whereas the long early morning plume tails result from rather slow transport. For example, with consistent winds of 0.5 m s^{-1}, air travel time is about 30 s and 1 h, respectively, at 15 m and 2 km downwind of freeway. Because traveling a transect with the MMP usually requires 10 to 15 min, and traffic flows on freeways often show patchy distributions, individual plume profiles are complicated to interpret due to different time scales between the peak and tails of plumes. For this reason, we use measurement period average profiles for the present study.

We note that the real-world problem addressed here is more complex than the simple case of dispersion from a steady line source. While UFP are a very good tracer for roadway pollutants, they do undergo a moderate amount of coagulation and evaporation/condensation on the time scales of interest here. Further, the line source is not steady; in the early morning the traffic density increases rapidly with time. Finally, the geometry of the intersection of the transect and the freeway varies among loca-

ACPD
13, 25253–25290, 2013

tions. The α and β values extracted as part of the semi-empirical treatment presented here account for all of these effects. Full theoretical treatments of all of the details of this problem are beyond the scope of this paper, and the results of our semi-empirical analysis may not agree completely with theoretical treatments of the simpler problem.

3 Results and discussions

3.1 Effectiveness of curve fit to the observations

For all four transects, curve fits provide excellent matches to the observed profiles of UFP number concentrations both at the peak and far downwind ($R^2 \sim 0.9$ or better) (Fig. 2). The fits do not explain slightly elevated UFP concentrations immediately upwind of the freeways. These elevations likely result from a combination of wind variability on a short timescale (or meandering behavior under calm conditions) and eddy diffusion in the direction opposite to the prevailing winds, neither of which is captured in the model.

Comparing α and β values for the averaged transects for all days provides an overview of how well the transects are described by the simple expression of dispersion parameters provided by the Briggs and other similar formulations. Day-to-day variability is discussed below. The mean values for α obtained from the transect-averaged UFP profiles were 0.07, 0.03, 0.02, and 0.03 for the DTLA, Paramount, Carson, and Claremont transects, respectively (Table 1). Briggs' (1973) values for α and β are also listed in Table 1. The mean α for the DTLA transect (0.07) is similar to the Briggs' value for urban areas under stable conditions ($\alpha = 0.08$), whereas α for the other three transects are comparable to the Briggs' constant for rural areas under moderately to slightly stable conditions ($\alpha = 0.02$–0.03). This is reasonable considering that the DTLA transect is in an area with scattered high buildings, while the other transects are predominately single story residential areas.

ACPD
13, 25253–25290, 2013

Observed mean β values were 0.4×10^{-3}, -0.5×10^{-3}, 0.6×10^{-3}, and 2.8×10^{-3} for DTLA, Paramount, Carson, and Claremont, respectively (Table 1), showing bigger differences from Briggs' β value. The mean β for the DTLA and Paramount transects were smaller than the Briggs' value for urban (1.5×10^{-3}) and rural areas (0.3×10^{-3}), respectively (if urban equation of Briggs' formula was used, $\beta = 1.1\times10^{-3}$ was obtained for DTLA). In contrast, β observed in Claremont was higher than the Briggs' β value. The Carson transect yielded a slightly higher β than Briggs' β value. Physically, these results suggest UFP emitted from freeways passing over the MMP transect (DTLA and Paramount) dispersed more quickly than anticipated by the Briggs 1973 analysis, while for Claremont they dispersed more slowly. Overall, both α and β varied widely by location when compared to the generalized Briggs' formula. Those differences might be caused in part by freeway topographic features (Wang and Zhang, 2009) and/or particle dynamic losses such as coagulation and evaporation (Zhang et al., 2004; Jacobson et al., 2005). Another possible contributor to those differences (particularly to β) is rapid temporal traffic changes during pre-sunrise periods. Traffic starts sharply increasing from 04:30 through 08:00 LT for the morning commute in the SoCAB, and observed UFP profiles result from both UFP freshly emitted near freeways and aged UFP in farther downwind areas, which were emitted about 1 h earlier when traffic was lighter. Hence, the observed profiles are expected to have lower β compared to those for constant emission sources. For DTLA and Paramount where β was significantly lower than Briggs' value, traffic increases from 1 h before the measurement period to the middle of the measurement period were significantly larger than those in Carson and Claremont (574 and 649 vehicles $\cdot$ 5 min^{-1} for DTLA and Paramount vs. 384 and 292 vehicles $\cdot$ 5 min^{-1} for Carson and Claremont, respectively). Nonetheless, β from observed profiles for the pre-sunrise period is meaningful in that: (1) traffic variations and corresponding ambient UFP profiles are typical for those periods, (2) traffic flow changes are very consistent ($1\sigma < 10$ %) among weekdays, and (3) concentrations farther downwind in plumes are the least influenced by emissions from freeways because they get close to background levels due to the dilution processes. In any case, the

ACPD
13, 25253–25290, 2013

curve fit methods provide an effective tool to estimate dispersion coefficients directly from the observations.

3.2 Impacts of dispersion coefficients and freeway-street interchange geometry on plume shapes

The dispersion coefficients α and β obtained from measurement period average concentration profiles show a strong positive correlation with one another, but clearly fall into two exclusive groups, apparently the result of the freeway-street interchange geometry (Fig. 3). Inputs in the curve fit equation (Eq. 2) for the two cases differ: source height $H = 6$ m for group A (freeway above transect) and $H = 0$ m for B (freeway below transect). Compared to group B, group A values for α ranged more widely and β varied less. For group A, it takes more time for the vehicular plume to reach the ground from the elevated freeway height, thus the location of the peak, which depends on α, may vary depending on topographic and atmospheric conditions. In contrast, for group B (underpass freeways), the peak will appear adjacent to the freeway regardless of atmospheric conditions because a plume rises directly from the freeway beneath, leading to smaller variations in α, and relatively larger variations in β.

A positive correlation between α and β suggests overlap in the factors that control them. Figure 1 illustrates that α is related to the peak position and plume width (advection), and β to plume dilution rates (eddy diffusion or entrainment). We can therefore hypothesize that the correlation between α and β is caused by (1) meteorological conditions (advection and turbulence; hypothesis 1) and/or (2) plume intensity (hypothesis 2). In the following sections, these two hypotheses are explored in detail.

3.3 Meteorological effects on plume characteristics (hypothesis 1: advection and dispersion)

Hypothesis 1 states that pollutants can be effectively advected farther with relatively moderate winds blowing steadily in one direction under stable conditions. Stronger

ACPD
13, 25253–25290, 2013

winds may produce more turbulence to disperse pollutants more rapidly. Thus, for stable pre-sunrise hours, moderate and consistent winds may be able to effectively transport plumes (smaller α), but would result in faster decay rates (smaller β), compared to weaker winds.

3.3.1 Wind direction

As expected, in addition to determining which side of the freeways downwind, wind direction was a determinant of plume length. The dispersion coefficient α, generally showed a negative relationship with wind direction relative to the freeway (WD_{rel}, 90° = normal to freeway), suggesting as expected that plumes are more effectively transported if winds are perpendicular to the freeway (Fig. 4a). A positive correlation between $\Delta[UFP]_{1\,km}$, the background subtracted UFP number concentration measured 1 km downwind of the freeway ($[UFP]_{1\,km} - [UFP]_{bkgnd}$) and WD_{rel} illustrates the effects of WD_{rel} on plume transport (Fig. 4b). However, the high scatter indicates the importance of other factors. The dispersion coefficient β is not correlated with WD_{rel} (not shown), because wind direction is not directly related to the dilution process.

3.3.2 Wind speed

At night, statically stable air suppresses turbulent energy production, thus under calm stable conditions, moderate consistent winds can help transport an air mass farther. Hypothesis 1 suggests that both α and β would decrease (more transport and faster dispersion) as wind speeds increase under calm conditions, assuming a consistent wind direction. α is likely to be more related to vector-averaged resultant wind speeds because the hypothesis concerns transport, whereas β should more depend on scalar wind speeds, which should most directly affect dispersion rates.

Figure 5a shows that α responds differently to resultant wind speeds (WSR) depending on freeway–street interchange geometry. Clear negative relationships between α and resultant wind speeds (WSR) were observed for the overpass freeway transects

ACPD
13, 25253–25290, 2013

(DTLA and Paramount, Fig. 5a). Different scales of α in DTLA and Paramount are likely to result from differences in land use (e.g., urbanized or semi-urbanized, see Sect. 3.1) and possibly from other factors (e.g., plume intensities caused by different traffic density, discussed below). Plumes emitted from the freeways above transects will be transported farther with higher resultant wind speeds before reaching the ground (smaller α), explaining the negative correlation between α and resultant wind speeds. In contrast, for the underpass freeways (Carson and Claremont), α appears to slightly increase with resultant wind speed, although the trend is largely driven by one data point obtained on 8 June 2011 (Fig. 5a). On that day, winds were unusually strong, the prevailing wind direction was reversed, and a fog formed in the downwind uphill area. For the underpass freeway transects, the peak concentration location might not be significantly influenced by wind speeds, since the MMP experienced a freshly emitted plume rising directly beneath the transect. Therefore, wind speeds might more strongly impact the dissipation rate (β) of a plume, creating faster decays and narrower peaks as the wind speed increases (Fig. 5b).

Scalar wind speeds (WSS) and β were, in general, negatively correlated when wind speeds were larger than $0.5\,\mathrm{m\,s^{-1}}$ particularly for the underpass freeways (Fig. 5b). In contrast to the α–WSR relationships, the overpass freeway transects were more weakly correlated than underpass freeway sites. It appears that wind speeds influence α more strongly for the overpass freeway transects, whereas for the underpass freeway transects β is more affected by wind speeds. This negative correlation is not valid under extremely light wind conditions (WSS $< 0.5\,\mathrm{m\,s^{-1}}$). Under these calm stable conditions, other parameters are likely to govern the dilution rate of a plume, such as concentration gradient (Sect. 3.4). Overall, within the small range of wind speed observed in early morning, winds alone are not the dominant factor in determining dispersion coefficients α and β under the stable pre-sunrise conditions. Consequently, hypothesis 1 by itself cannot explain entirely the variations in plume decays.

ACPD
13, 25253–25290, 2013

3.4 Effects of freeway emissions on plume extension (hypothesis 2: dilution and entrainment)

Hypothesis 2 states that more intensive plumes can decay faster due to larger concentration gradients between background and plume. Dillon et al. (2002) and LaFranchi et al. (2011) used Eq. (4) to express dilution rates during urban plume transport, and Choi et al. (2012) showed that a dilution rate coefficient (K) near the peak of freeway plumes can be determined by integrating Eq. (4):

$$\frac{\mathrm{d}([C]_t - [C]_{\mathrm{bkgnd}})}{\mathrm{d}t} = -K \cdot ([C]_t - [C]_{\mathrm{bkgnd}}) \quad (4)$$

where t is time, $[C]_t$ and $[C]_{\mathrm{bkgnd}}$ are pollutant concentrations at time t in the plume and in the background, respectively. Because the dilution rate is a function of $\Delta[C]$ between the background and plume as well as the dilution rate coefficient (K), differences in decay rates of individual pollutants and among UFP numbers for different size bins can be observed even in the same plume if concentration profiles were normalized only by peak or background (Karner et al., 2010; Choi et al., 2012). In addition, because Δ[UFP] decreases with distance, the decay rate is dampened as a plume is diluted. This pattern is clearly shown in the observed spatial profiles of UFP for all transects (Fig. 2).

3.4.1 Effects of Δ[UFP] on plume decay rates

$\Delta[\mathrm{UFP}]_{\mathrm{peak}}$, defined as the differences between the background and plume peak concentrations, showed clear and consistent negative correlations with both the dispersion coefficients α and β (Fig. 6a and b), in contrast to wind speed and direction. As shown in Sect. 2.3.2 (Fig. 1a), more intense plumes tend to have lower α values, explaining the negative correlation between α and $\Delta[\mathrm{UFP}]_{\mathrm{peak}}$. Although α and $\Delta[\mathrm{UFP}]_{\mathrm{peak}}$ seem to follow a single trend line, the transects populate different parts of the curve, with larger $\Delta[\mathrm{UFP}]_{\mathrm{peak}}$ corresponding to the underpass freeway transects.

ACPD
13, 25253–25290, 2013

Due to different slopes in these two groups, the overall trend line has an exponential form ($\alpha = 0.14 \cdot \exp(-3.64 \times 10^{-5}\,\Delta[\mathrm{UFP}])$, $R^2 = 0.59$).

Dependencies of β on $\Delta[\mathrm{UFP}]_{\mathrm{peak}}$ fall into two groups corresponding to freeway-street interchange geometry, as discussed in Sect. 3.2 (Fig. 6b). The negative correlation between β and $\Delta[\mathrm{UFP}]_{\mathrm{peak}}$ is consistent with hypothesis 2, as β appears to be a parameter related to plume dissipation (Sect. 2.3.2, Fig. 1b). For these reasons, we conclude the decay rates are strongly influenced by not only wind speed and direction but also the concentration difference relative to the background, i.e. $\Delta[\mathrm{UFP}]_{\mathrm{peak}}$.

3.4.2 Temperature, atmospheric stability, and emission factor

Although temperature does not directly affect the dissipation rates of plumes, we found a clear positive correlation between the temperature and the dispersion coefficient, α (Fig. 7b). Because higher UFP emissions from vehicle tailpipes are strongly related to colder temperatures, particularly for the nucleation mode (10–20 nm) (Kittelson et al., 2004, 2001; Morawska et al., 2005), colder temperatures might indirectly lower dispersion coefficients by elevating UFP concentrations from vehicular sources, and hence increasing $\Delta[\mathrm{UFP}]_{\mathrm{peak}}$ (Fig. 6a). Consistent with this explanation and supporting the emissions studies (Kittelson et al., 2004, 2001; Morawska et al., 2005), higher $\Delta[\mathrm{UFP}]_{\mathrm{peak}}$ values normalized to the traffic density were indeed observed at lower ambient temperatures for all transects (Fig. 7b). Zhu et al. (2006) also showed the same inverse relationship between temperature and UFP concentrations corrected for traffic volume at the edge of the I-405 freeway.

The Richardson number (Ri) is a common indicator of atmospheric stability. It combines the vertical temperature gradient (static stability) with mechanical wind shear (Stull, 1988) as expressed in Eq. (5):

$$\text{Richardson number, } Ri \equiv \frac{g}{\overline{\theta}} \frac{\mathrm{d}\theta}{\mathrm{d}z} \cdot \left(\frac{\mathrm{d}U}{\mathrm{d}z} \right)^{-2} \tag{5}$$

ACPD
13, 25253–25290, 2013

where $\overline{\theta}$ is the mean potential temperature in the layer, $d\theta \cdot dz^{-1}$ is temperature gradient, $dU \cdot dz^{-1}$ is vertical wind shear, and g is the gravitational acceleration ($R_i > 0$ for stable; $Ri = 0$ for neutral; and Ri < 0 for unstable air). Ri values for all transects fell in the near neutral to stable ranges during the pre-sunrise periods (Fig. 8). Background UFP concentrations tend to increase when air is more stable (Fig. 8a) as expected. However, the decay rate coefficient β appears to decrease (the plume dissipates more rapidly) when the nocturnal atmosphere is more stable (Fig. 8b). We interpret this phenomenon as a result of hypothesis 2; a larger $\Delta[\mathrm{UFP}]_{\mathrm{peak}}$ under more stable conditions leads to a faster dissipation rate in a plume as discussed above.

Consequently, the effects of temperature and atmospheric stability on plume dissipation rates further support the importance of hypothesis 2 for plume decay rates. Nonetheless, we should emphasize that faster decay rates do not necessarily mean reduced plume impacts because faster dissipations were observed for higher $\Delta[\mathrm{UFP}]_{\mathrm{peak}}$ conditions, and higher peak concentrations eventually lead to more elevated UPF concentrations in the far downwind areas (e.g., $\Delta[\mathrm{UFP}]_{\mathrm{peak}}$ shows a positive correlation with Δ[UFP] at 1500 m downwind from the freeway; not shown).

3.5 Estimate of particle number emission factor

Vehicular emissions from the freeways depend on traffic volumes, fleet composition and maintenance, driving conditions, and fuel composition (e.g., sulfur content) (Kumar et al., 2011). Emission rates of UFP estimated by a number of previous studies show considerable variability (Kumar et al., 2011). The freeways studied here have similar vehicle composition with modest contributions from heavy-duty vehicles (< 3–7 %), and consistent traffic speeds due to lower traffic densities during the pre-sunrise periods. Thus, it is expected that traffic volume is a dominant factor in controlling the variations in emission rates from the freeways. Figure 9a shows a strong linear relationship between the emission parameter, Q_c and traffic density during the measurement periods, at least when traffic flow ranged from 400 to 1200 vehicles $\cdot$ 5 min^{-1}, further supporting

ACPD
13, 25253–25290, 2013

the effectiveness of the curve fit methods described here, including the ability of Q_c to describe vehicular emission rates from the freeways.

With the mean Q_c (8.12×10^4 particles $\cdot$ m cm^{-3}), observed wind speeds (0.64 m s^{-1}), a wind speed correction factor due to traffic wake suggested by Chock (1978) for stable air (0.2 m s^{-1}), and observed traffic flows on freeways (680 vehicles $\cdot$ 5 min^{-1}), the mean particle number emission factor (PNEF), q_{veh}, can be estimated from Eq. (6):

$$q_{veh} = \frac{\sqrt{2\pi} Q_c \cdot U_e}{(\text{traffic density})} = \frac{\sqrt{2\pi} \times (8.12 \times 10^4 \,\#\cdot \text{m cm}^{-3}) \times (0.64 + 0.2\,\text{m s}^{-1}) \times 10^6\,\text{cm}^3\,\text{m}^{-3} \times 300\,\text{s} \cdot 5\,\text{min}^{-1}}{(680.2\,\text{vehicles} \cdot 5\,\text{min}^{-1})} \quad (6)$$

where the last two values of the numerator are unit conversion factors. This estimate is for "survived" UFP through the very early stage of vigorous mixing/particle dynamics occurring within 1–3 s of initial emissions from tailpipes (Zhang and Wexler, 2004). The averaged q_{veh} for a mixed fleet on the 101, 91, I-110, and I-210 freeways with consistent fleet speeds under stable pre-sunrise conditions was estimated as $1.2(\pm 0.6) \times 10^{14}$ particles $\cdot$ vehicle^{-1} mi^{-1}, which is smaller than the estimate (8.3×10^{14} particles $\cdot$ vehicle^{-1} mi^{-1}) made in a similar manner by Zhu and Hinds (2005) for the nearby I-405 freeway in 2001. Although our PNEF estimate does not consider the initial stage on tailpipe-to-road scale (Zhang and Wexler, 2004), we note (1) the "survived" ultrafines can potentially affect human exposures and urban aerosol budgets on road-to-ambient scale and (2) ambient conditions under which measurements were conducted were representative of stable pre-sunrise periods generally found in the SoCAB with respect to traffic patterns/composition and surface meteorology. We also note the previous estimate made in 2001 (Zhu and Hinds, 2005) did not consider detailed particle dynamics, so that comparison between the two studies is appropriate.

In Choi et al. (2012), we also reported reduced peak UFP concentrations near freeways compared to the peak values observed in 2008 and 2005 by Hu et al. (2009)

ACPD
13, 25253–25290, 2013

and Zhu et al. (2006), respectively. In addition, Quiros et al. (2013) reported a value of PNEF (6.0×10^{13} particles vehicle^{-1} mi^{-1}) consistent to our estimate. Between 2001 and 2010, many characteristics of the vehicle fleet have changed, such as improvement of engine emissions control technology, fleet turnover to newer cleaner vehicles, recent shifts to smaller engines (Snyder, 2011), and more stringent regulations for truck engines and fuel composition by the California Air Resources Board (CARB, 2008, 2004) as discussed in Quiros et al. (2013).

3.6 Predicting plume behavior

Accurate prediction of plume peak heights and extents without the use of highly specialized data is clearly desirable. If we can properly estimate Q_c, α, and β (Eq. 2), the Gaussian line source model can accurately predict not only the peak concentration but also the extension of the plumes. Here, we use a multivariate linear regression method to reproduce plume parameters (Q_c, α and β). Because plume peak concentration determined by Q_c, is an important parameter controlling the dispersion coefficients α and β (Sect. 3.4.1), we found the best results by first, estimating Q_c from various related factors, and then adding Q_c as a predictor variable in multivariate regression analysis for α and β as discussed below.

For Q_c estimation, traffic flows, wind direction, wind speeds, temperature, relative humidity were used as predictor variables based on theoretical and observed (measurement period average) relationships between ΔUFP and predictor variables (Eq. 7):

$$Q_{c,j} = \mathrm{coef}_1 \cdot \mathrm{TF}_j + \mathrm{coef}_2 \cdot \left|\mathrm{WD}_{\mathrm{rel},j}\right| + \mathrm{coef}_3 \cdot \mathrm{WSR}_j + \mathrm{coef}_4 \cdot T_j + \mathrm{coef}_5 \cdot \mathrm{RH}_j + C \quad (j = 1, 2, 3, \ldots, k) \tag{7}$$

where j indicates the jth observation, and TF, $\mathrm{WD}_{\mathrm{rel}}$, WSR, T, RH, and C are the traffic flows (vehicles · 5 min^{-1}), wind direction relative to the freeway orientation (°), ambient temperature (°C), resultant wind speed (m s^{-1}), relative humidity (%), and a correction factor, respectively. Similarly, α (for overpass freeways) and β (for underpass freeways)

ACPD
13, 25253–25290, 2013

were obtained from the observed meteorological and emission data (Q_c) (Eq. 8):

$$\alpha_j \text{ or } \beta_j = \text{coef}_1 \cdot Q_{c,j} + \text{coef}_2 \cdot \left|\text{WD}_{\text{rel},j}\right| + \text{coef}_3 \cdot T_j + \text{coef}_4 \cdot \text{WSR}_j + \text{coef}_5 \cdot \text{RH}_j + C \quad (j = 1, 2, 3, \ldots, k) \tag{8}$$

In this analysis observed Q_c was used as an input parameter rather than estimated Q_c from Eq. (7) to avoid multivariate regression error. Regressions were performed separately according to freeway topography because as discussed earlier α varied more widely for overpass freeways and β had a wider range for underpass freeways (Fig. 3). In addition, there were different dependencies of dispersion parameters on WSR and Q_c (Figs. 5a and 9b) for the two interchange geometries.

Calculated coefs, and resulting R^2 and p values for both Q_c, α and β are listed in Table 3. For Q_c, temperature and traffic were important parameters for both overpass and underpass freeways, while wind speed and wind direction were important only for overpass freeways and underpass freeways, respectively. The inverse sign for coef_1 (traffic flows) against observations was likely due to multicollinearity effects between predictor parameters (O'brien, 2007). Although multicollinearity is detrimental to estimating the comparative importance of individual explanatory parameters, it does not reduce prediction validity or reliability of regression results as a whole (Lipovetsky and Conklin, 2001), The resulting Q_c from multivariate regression showed good agreement with observations with overall R^2 of 0.95.

Dispersion coefficients were most sensitive to Q_c and least sensitive to T for both freeway geometries. Although RH by itself was poorly correlated with α and β, it showed modest importance in multivariate regressions. As noted, α and β showed strong positive correlations with one another, once separated for interchange geometry (Fig. 3; Eqs. 9 and 10):

$$\beta = 3.45 \times 10^{-2}\alpha - 1.64 \times 10^{-3} \quad (R^2 = 0.90) \quad \text{for group A (overpass freeways)} \tag{9}$$

$$\alpha = 5.37\beta + 1.93 \times 10^{-2} \quad (R^2 = 0.74) \quad \text{for group B (underpass freeways)} \tag{10}$$

ACPD
13, 25253–25290, 2013

Thus, from appropriately estimated α or β from multivariate regressions, we could further obtain β or α using Eqs. (9) and (10). Overall, resulting values of α and β from multivariate regression analyses showed good agreement with observations with R^2 = 0.88 and 0.86 for overpass and underpass freeways, respectively (Fig. 10).

Despite successful application of multivariate regression, we note that input data points (13 for underpass freeways and 10 for overpass freeways) were not sufficient compared to the number of predictor variables in this multivariate regression analysis. Specifically, the effects of land-use on α variations for overpass freeway transects, if any, were not considered in this analysis, but land-use effects are considered an important factor to parameterize α in Briggs' formula in addition to stability class (Table 1). Thus, further measurements are needed to verify these results. Nonetheless, we believe this method provides a more efficient and precise tool to predict freeway plume profiles near major roadways under stable conditions compared with conventional simple formulas for dispersion coefficients. This study also provides useful datasets and the potential to parameterize dispersion coefficients and emission factors for more sophisticated model simulations.

Acknowledgements. The authors gratefully acknowledge support for this study by the California Air Resources Board, Contract No. 09–357. The mobile monitoring platform measurements were made possible with the generous assistance of our colleagues: Meilu He, Kathleen Kozawa, Steve Mara, and Vincent Barbesant.

References

Briant, R., Korsakissok, I., and Seigneur, C.: An improved line source model for air pollutant dispersion from roadway traffic, Atmos. Environ., 45, 4099–4107, 2011.

Briggs, G. A.: Diffusion Estimation for Small Emissions, NOAA, Oak Ridge, TN, 1973.

Capaldo, K. and Pandis, S.: Lifetimes of Ultrafine Diesel Aerosol, Carnegie Mellon University, Pittsburgh, PA, 2001.

CARB: The California Diesel Fuel Regulations, California Air Resources Board, Sacramento, available at: http://www.arb.ca.gov/fuels/diesel/diesel.htm (last access: 12 May 2012), 2004.

ACPD

13, 25253–25290, 2013

CARB: Amendments to Adopt More Stringent Emission Standards for 2007 and Subsequent Model Year New Heavy-Duty Diesel Engines, California Air Resources Board, Sacramento, 2008.
Chen, H., Bai, S., Eisinger, D., Niemeier, D., and Claggett, M.: Predicting Near-Road $PM_{(2.5)}$ Concentrations Comparative Assessment of CALINE4, CAL3QHC, and AERMOD, Transp. Res. Record, 2123, 26–37, doi:10.3141/2123-04, 2009.
Chock, D. P.: Simple line-source model for dispersion near roadways, Atmos. Environ., 12, 823–829, 1978.
Choi, W. and Paulson, S. E.: Evolution of nanoparticles with distance travelled from the major roads under stable pre-sunrise conditions, in preparation, 2013.
Choi, W., He, M., Barbesant, V., Kozawa, K. H., Mara, S., Winer, A. M., and Paulson, S. E.: Prevalence of wide area impacts downwind freeways under pre-sunrise stable atmospheric conditions, Atmos. Environ., 62, 318–327, doi:10.1016/j.atmosenv.2012.07.084, 2012.
Dillon, M. B., Lamanna, M. S., Schade, G. W., Goldstein, A. H., and Cohen, R. C.: Chemical evolution of the Sacramento urban plume: transport and oxidation, J. Geophys. Res.-Atmos., 107, 4045, doi:10.1029/2001jd000969, 2002.
Gramotnev, G., Brown, R., Ristovski, Z., Hitchins, J., and Morawska, L.: Determination of average emission factors for vehicles on a busy road, Atmos. Environ., 37, 465–474, doi:10.1016/s1352-2310(02)00923-8, 2003.
Hoek, G., Boogaard, H., Knol, A., De Hartog, J., Slottje, P., Ayres, J. G., Borm, P., Brunekreef, B., Donaldson, K., Forastiere, F., Holgate, S., Kreyling, W. G., Nemery, B., Pekkanen, J., Stone, V., Wichmann, H. E., and Van der Sluijs, J.: Concentration response functions for ultrafine particles and all-cause mortality and hospital admissions: results of a European expert panel elicitation, Environ. Sci. Technol., 44, 476–482, doi:10.1021/es9021393, 2010.
Hu, S. S., Fruin, S., Kozawa, K., Mara, S., Paulson, S. E., and Winer, A. M.: A wide area of air pollutant impact downwind of a freeway during pre-sunrise hours, Atmos. Environ., 43, 2541–2549, doi:10.1016/j.atmosenv.2009.02.033, 2009.
Hussein, T., Karppinen, A., Kukkonen, J., Harkonen, J., Aalto, P. P., Hameri, K., Kerminen, V. M., and Kulmala, M.: Meteorological dependence of size-fractionated number concentrations of urban aerosol particles, Atmos. Environ., 40, 1427–1440, doi:10.1016/j.atmosenv.2005.10.061, 2006.

ACPD
13, 25253–25290, 2013

Jacobson, M. Z., Kittelson, D. B., and Watts, W. F.: Enhanced coagulation due to evaporation and its effect on nanoparticle evolution, Environ. Sci. Technol., 39, 9486–9492, doi:10.1021/es0500299, 2005.

Karner, A. A., Eisinger, D. S., and Niemeier, D. A.: Near-roadway air quality: synthesizing the findings from real-world data, Environ. Sci. Technol., 44, 5334–5344, doi:10.1021/es100008x, 2010.

Kerminen, V. M., Pakkanen, T. A., Makela, T., Hillamo, R. E., Sillanpaa, M., Ronkko, T., Virtanen, A., Keskinen, J., Pirjola, L., Hussein, T., and Hameri, K.: Development of particle number size distribution near a major road in Helsinki during an episodic inversion situation, Atmos. Environ., 41, 1759–1767, doi:10.1016/j.atmosenv.2006.10.026, 2007.

Kittelson, D. B., Watts, W. F., and Johnson, J. P.: Fine Particle (Nanoparticle) Emissions on Minnesota Highways, Final Report, Minnesota Department of Transportation, 2001.

Kittelson, D. B., Watts, W. F., and Johnson, J. P.: Nanoparticle emissions on Minnesota highways, Atmos. Environ., 38, 9–19, doi:10.1016/j.atmosenv.2003.09.037, 2004.

Knol, A. B., de Hartog, J. J., Boogaard, H., Slottje, P., van der Sluijs, J. P., Lebret, E., Cassee F. R., Wardekker, J. A., Ayres, J. G., Borm, P. J., Brunekreef, B., Donaldson, K., Forastiere, F., Holgate, S.T., Kreyling, W. G., Nemery, B., Pekkanen, J., Stone, V., Wichmann, H. E., and Hoek, G.: Expert elicitation on ultrafine particles: likelihood of health effects and causal pathways, Particle Fibre Toxicol., 6, 1, doi:10.1186/1743-8977-6-19, 2009.

Kozawa, K. H., Fruin, S. A., and Winer, A. M.: Near-road air pollution impacts of goods movement in communities adjacent to the Ports of Los Angeles and Long Beach, Atmos. Environ., 43, 2960–2970, doi:10.1016/j.atmosenv.2009.02.042, 2009.

Kumar, P., Robins, A., Vardoulakis, S., and Britter, R.: A review of the characteristics of nanoparticles in the urban atmosphere and the prospects for developing regulatory controls, Atmos. Environ., 44, 5035–5052, doi:10.1016/j.atmosenv.2010.08.016, 2010.

Kumar, P., Ketzel, M., Vardoulakis, S., Pirjola, L., and Britter, R.: Dynamics and dispersion modelling of nanoparticles from road traffic in the urban atmospheric environment – a review, J. Aerosol. Sci., 42, 580–603, doi:10.1016/j.jaerosci.2011.06.001, 2011.

LaFranchi, B. W., Goldstein, A. H., and Cohen, R. C.: Observations of the temperature dependent response of ozone to NO_x reductions in the Sacramento, CA urban plume, Atmos. Chem. Phys., 11, 6945–6960, doi:10.5194/acp-11-6945-2011, 2011.

Lipovetsky, S. and Conklin, M.: Analysis of regression in game theory approach, Appl. Stoch. Model. Bus., 17, 319–330, doi:10.1002/asmb.446, 2001.

ACPD
13, 25253–25290, 2013

Luhar, A. K. and Patil, R. S.: A general finite line source model for vehicular pollution prediction, Atmos. Environ., 23, 555–562, 1989.
Moller, P., Folkmann, J. K., Forchhammer, L., Brauner, E. V., Danielsen, P. H., Risom, L., and Loft, S.: Air pollution, oxidative damage to DNA, and carcinogenesis, Cancer Lett., 266, 84–97, doi:10.1016/j.canlet.2008.02.030, 2008.
Morawska, L., Jamriska, M., Thomas, S., Ferreira, L., Mengersen, K., Wraith, D., and McGregor, F.: Quantification of particle number emission factors for motor vehicles from on-road measurements, Environ. Sci. Technol., 39, 9130–9139, doi:10.1021/es050069c, 2005.
O'brien, R. M.: A caution regarding rules of thumb for variance inflation factors, Qual. Quant., 41, 673–690, doi:10.1007/s11135-006-9018-6, 2007.
Pasquill, F.: The estimation of the dispersion of windborne material, Meteorol. Mag., 90, 33–49, 1961.
Pey, J., Querol, X., Alastuey, A., Rodriguez, S., Putaud, J. P., and Van Dingenen, R.: Source apportionment of urban fine and ultra-fine particle number concentration in a western mediterranean city, Atmos. Environ., 43, 4407–4415, doi:10.1016/j.atmosenv.2009.05.024, 2009.
Quiros, D. C., Zhang, Q., Choi, W., He, M., Paulson, S. E., Winer, A. M., Wang, R., and Zhu, Y. F.: Near-roadways air quality impacts of a scheduled 36-hour closure of a major highway, Atmos. Environ., 67, 404–414, doi:10.1016/j.atmosenv.2012.10.020, 2013.
Sharan, M. and Yadav, A. K.: Simulation of diffusion experiments under light wind, stable conditions by a variable K-theory model, Atmos. Environ., 32, 3481–3492, doi:10.1016/s1352-2310(98)00048-x, 1998.
Sharma, P. and Khare, M.: Modelling of vehicular exhausts – a review, Transport. Res. D-Tr. E, 6, 179–198, doi:10.1016/s1361-9209(00)00022-5, 2001.
Stull, R. B.: An Introduction to Boundary Layer Meteorology, Kluwer Academic Publishers, Dordrecht, the Netherlands, 1988.
Wang, Y. J. and Zhang, K. M.: Modeling near-road air quality using a computational fluid dynamics model, CFD-VIT-RIT, Environ. Sci. Technol., 43, 7778–7783, doi:10.1021/es9014844, 2009.
Westerdahl, D., Fruin, S., Sax, T., Fine, P. M., and Sioutas, C.: Mobile platform measurements of ultrafine particles and associated pollutant concentrations on freeways and residential streets in Los Angeles, Atmos. Environ., 39, 3597–3610, doi:10.1016/j.atmosenv.2005.02.034, 2005.

ACPD
13, 25253–25290, 2013

Zhang, K. M. and Wexler, A. S.: Evolution of particle number distribution near roadways – Part I: Analysis of aerosol dynamics and its implications for engine emission measurement, Atmos. Environ., 38, 6643–6653, doi:10.1016/j.atmosenv.2004.06.043, 2004.

Zhang, K. M., Wexler, A. S., Zhu, Y. F., Hinds, W. C., and Sioutas, C.: Evolution of particle number distribution near roadways. Part II: The "road-to-ambient" process, Atmos. Environ., 38, 6655–6665, doi:10.1016/j.atmosenv.2004.06.044, 2004.

Zhu, Y. F. and Hinds, W. C.: Predicting particle number concentrations near a highway based on vertical concentration profile, Atmos. Environ., 39, 1557–1566, 2005.

Zhu, Y. F., Kuhn, T., Mayo, P., and Hinds, W. C.: Comparison of daytime and nighttime concentration profiles and size distributions of ultrafine particles near a major highway, Environ. Sci. Technol., 40, 2531–2536, 2006.

ACPD
13, 25253–25290, 2013

Table 1. Parameterizations of σ_z for Gaussian and K-theory dispersion models and σ_z values obtained from transect averaged ultrafine particle concentration profiles in this study.

References	Equation form	Land use	Stability class	σ_z or γ[b] formula	
Chock (1978)	$\sigma_z = (a + b \cdot x)^c$	N/A	Stable	$a = 1.49$, $b = 0.15$, $c = 0.77$	
Briggs (1973)	$\sigma_z = \frac{\alpha \cdot x}{1+\beta \cdot x}$	Rural	E[a] (slightly stable)	$\alpha = 0.03$ $\beta = 0.3 \times 10^{-3}$	
			F[a] (moderately stable)	$\alpha = 0.016$ $\beta = 0.3 \times 10^{-3}$	
	$\sigma_z = \frac{\alpha \cdot x}{\sqrt{1+\beta \cdot x}}$	Urban	E–F[a] (stable)	$\alpha = 0.08$ $\beta = 1.5 \times 10^{-3}$	
Sharan and Yadav (1998)	$\gamma = (\sigma_w / U)^2$	N/A	Stable or unstable	$\sigma_w = \sqrt{\overline{(w - \overline{w})^2}}$	
This study (transect averaged σ_z and R^2 for curve fit)	$\sigma_z = \frac{\alpha \cdot x}{1+\beta \cdot x}$	Urban to sub-urban	Near neutral to stable pre-sunrise periods	DTLA ($R^2 = 0.96$)	$\alpha = 0.07$ $\beta = 0.4 \times 10^{-3}$
				Paramount ($R^2 = 0.96$)	$\alpha = 0.034$ $\beta = -4.6 \times 10^{-4}$
				Carson ($R^2 = 0.91$)	$\alpha = 0.02$ $\beta = 0.6 \times 10^{-3}$
				Claremont ($R^2 = 0.87$)	$\alpha = 0.03$ $\beta = 2.8 \times 10^{-3}$

[a] D, E, and F are Pasquill stability classes for nighttime conditions (Pasquill, 1961).

[b] γ represents a turbulence parameter used in Sharan and Yadav (1998), where σ_w is turbulence intensity in vertical direction, w is vertical wind component, and U is the mean wind speed.

ACPD
13, 25253–25290, 2013

Table 2. Summary of measurements, estimated emission parameters, Q_c, and dispersion coefficients (α and β) from the curve fits.

Sampling area (transect street)	Date	Backgnd[a] conc. ($\times 10^3$)	Q_c ($\times 10^4$)	α	β ($\times 10^{-3}$)	Model fit condition
Downtown LA (Coronado St.)	24 Feb 2011	16.1	1.34	0.059	0.81	$H = 6$ m
	7 Mar 2011	4.7	0.93	0.105	1.79	$z = 1.5$ m
	9 Mar 2011	14.7	0.99	0.056	0.15	
	14 Mar 2011	13.0	1.15	0.085	1.72	
	17 Mar 2011	16.1	0.63	0.089	1.21	
Paramount (Obispo St.)	27 Jan 2011	19.3	1.86	0.038	−0.19	$H = 6$ m
	1 Feb 2011	18.3	1.83	0.045	−0.12	$z = 1.5$ m
	10 Mar 2011	12.4	1.32	0.048	−0.34	
	15 Mar 2011	6.1	1.70	0.063	0.58	
	18 Mar 2011	19.8	1.94	0.038	−0.43	
West Carson (228th St.)	21 Jan 2011	23.6	0.63	0.024	1.29	$H = 0$ m[b]
	3 Feb 2011	21.6	0.74	0.016	0.09	$z = 1.5$ m
	8 Mar 2011	11.0	0.43	0.034	1.51	
	11 Mar 2011	14.2	0.56	0.020	−0.14	
	16 Mar 2011	15.3	0.27	0.035	3.85	
	29 Mar 2011	12.3	0.58	0.023	0.14	
Claremont (Mountain Ave.)	19 May 2011	4.8	0.38	0.030	3.42	$H = 0$ m[b]
	24 May 2011	6.4	0.26	0.035	5.37	$z = 1.5$ m
	25 May 2011	7.2	0.32	0.066	7.29	
	26 May 2011	7.0	0.39	0.020	1.44	
	1 Jun 2011	5.1	0.31	0.050	5.18	
	2 Jun 2011	7.4	0.50	0.029	2.27	
	7 Jun 2011	7.1	0.26	0.048	4.55	

[a] Background concentrations are defined as a lower 25 % quantile point in the upwind area.
[b] Actual height of the freeway surface is about 6 m below the transect. However, it is assumed that a freeway plume is well mixed within freeway area due to mechanical turbulence produced by vehicle wakes and then rolls up to the measurement transect.

ACPD
13, 25253–25290, 2013

Table 3. Coefficients for α (for overpass freeways) and β (for underpass freeways) obtained from multivariate linear regression using Eq. (8). Bold fonts represent the dominant contributors in the analyses.

	Emission factor Q_c		Dispersion coefficients	
	Overpass FWY (DTLA and Paramount)	Underpass FWY (Carson and Mountain)	α (Overpass FWY)	β (Underpass FWY)
$coef_1$	-2.1×10^2	**55.7**	$\mathbf{-4.4 \times 10^{-7}}$	$\mathbf{-1.7 \times 10^{-7}}$
$coef_2$	-5.8×10^2	$\mathbf{5.2 \times 10^2}$	3.5×10^{-4}	-8.7×10^{-5}
$coef_3$	$\mathbf{-1.8 \times 10^5}$	-2.3×10^4	-3.3×10^{-2}	$\mathbf{-1.3 \times 10^{-2}}$
$coef_4$	$\mathbf{-3.9 \times 10^4}$	$\mathbf{-1.2 \times 10^3}$	3.7×10^{-3}	-1.2×10^{-4}
$coef_5$	-8.3×10^2	-31.7	$\mathbf{7.1 \times 10^{-4}}$	-8.1×10^{-5}
C	9.8×10^5	9.8×10^4	2.3×10^{-2}	2.8×10^{-2}
R^2	0.84 (0.092)	0.75 (0.042)	0.91 (0.032)	0.81 (0.018)
(p value)	Overall R^2 = 0.95			

ACPD
13, 25253–25290, 2013

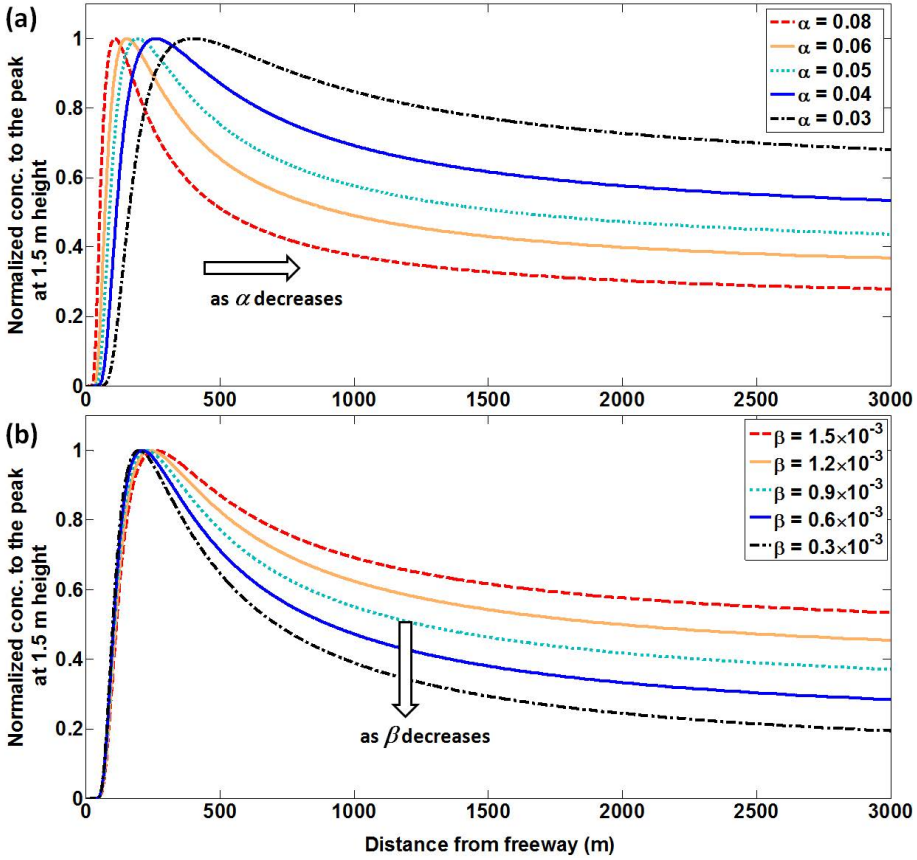

Fig. 1. Variations in spatial profiles of pollutants calculated with Eqs. (2) and (3) varying α or β. X axis is distance downwind from freeway and y axis is normalized concentrations to the peak at 1.5 m height ($z = 1.5$ m). Results were obtained **(a)** with fixed Q_c and $\beta = 1.5 \times 10^{-3}$ and varying α from 0.03 to 0.08, and **(b)** with a fixed Q_c and $\alpha = 0.04$, changing β from 0.3–1.5×10^{-3}.

ACPD
13, 25253–25290, 2013

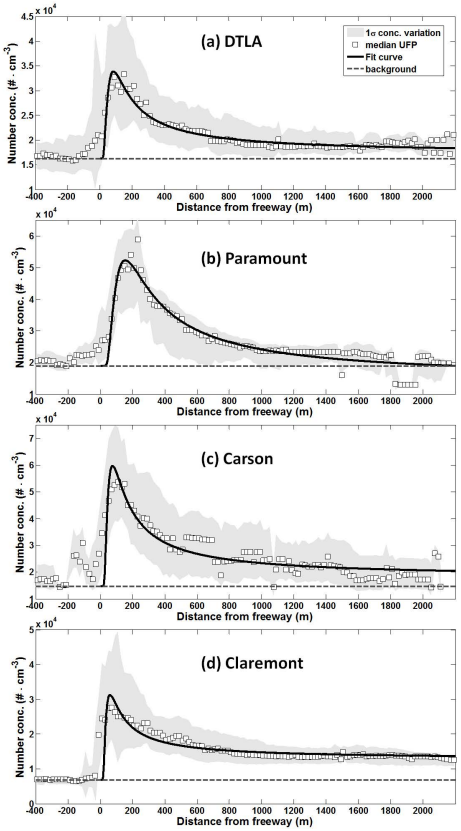

Fig. 2. Observed median UFP number concentrations with distance downwind of freeways (white squares), 1σ variation ranges (gray areas), upwind background concentrations (horizontal gray dashed lines), and curve fits to the observations with Gaussian dispersion model form (black lines) for transects at **(a)** DTLA, **(b)** Paramount, **(c)** Carson, and **(d)** Claremont.

ACPD
13, 25253–25290, 2013

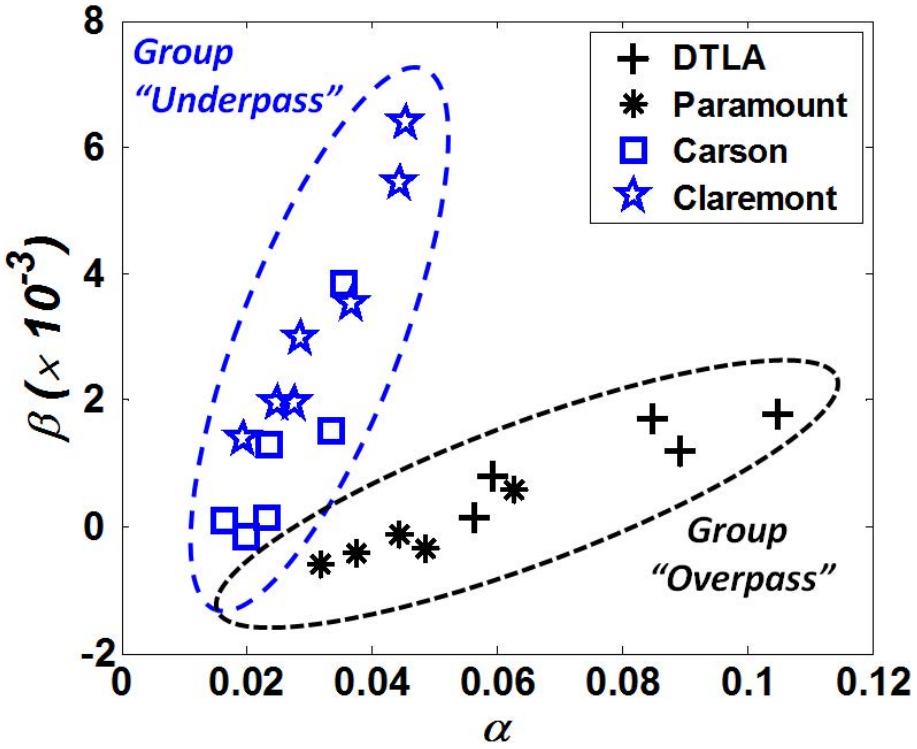

Fig. 3. Relationship between α and β obtained from the curve fits to daily mean spatial profiles of UFP in the DTLA (black crosses), Paramount (black asterisks), Carson (blue squares), and Claremont (blue stars) transects. Black dotted line represents a group A, where freeways overpass the transects and blue dashed line a group B, where freeways pass under the transects.

ACPD
13, 25253–25290, 2013

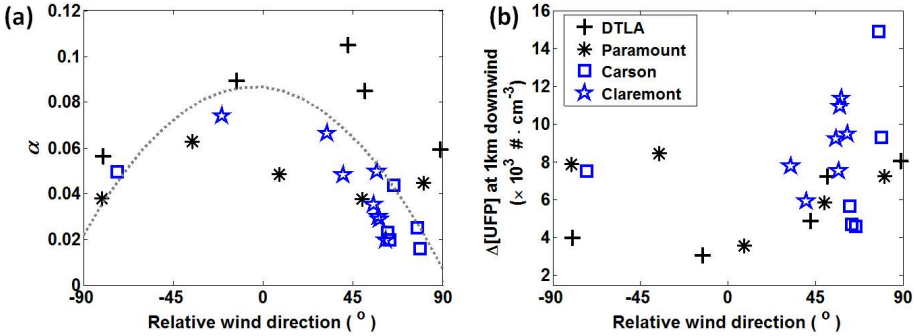

Fig. 4. Wind direction effects on **(a)** dispersion coefficient, α, and **(b)** background subtracted UFP concentrations at 1 km downwind of freeway. Black crosses, black asterisks, blue squares, and blue stars represent daily mean values for the DTLA, Paramount, Carson, and Claremont transects, respectively. Relative wind direction is daily mean wind direction relative to freeway orientation (90° = normal to freeway). Gray dotted line in **(a)** represents 2nd order polynomial fits (R^2 = 0.48).

ACPD
13, 25253–25290, 2013

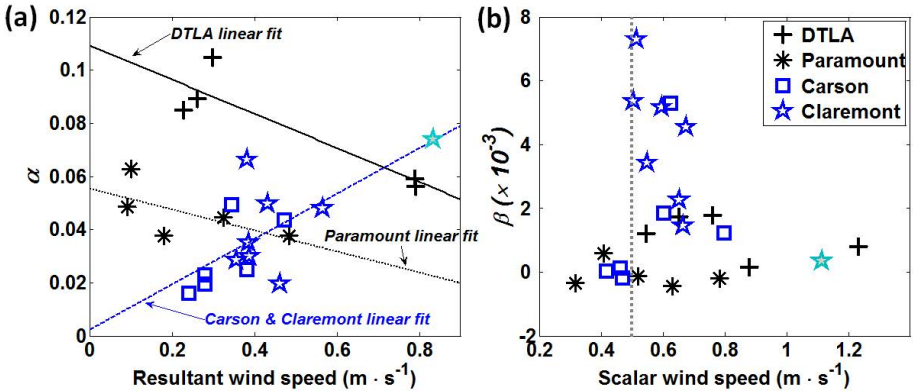

Fig. 5. Variations in dispersion coefficients as a function of wind speeds. **(a)** α vs. vector averaged resultant wind speeds. **(b)** β vs. scalar averaged wind speeds. Black solid line is a linear fit for the DTLA data points, black dotted line for Paramount, and blue dash-dotted line for Carson and Claremont. Vertical dotted line in **(b)** represents scalar wind speed of 0.5 m s^{-1}. Light blue star denotes Claremont data obtained on 8 June 2011 when wind was strong with reversed prevailing wind direction and fogs in the uphill downwind area.

ACPD
13, 25253–25290, 2013

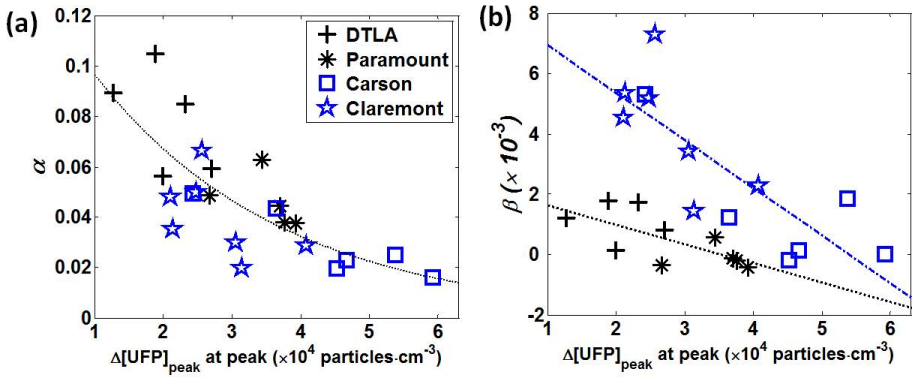

Fig. 6. Plots of the relationships of concentration gradient ($\Delta[\mathrm{UFP}]_{\mathrm{peak}}$) at the peak with **(a)** α and **(b)** β. Dotted lines in plot **(a)** is an exponential curve fits: $\alpha = 0.14 \cdot \exp(-3.64 \times 10^{-5} \cdot \Delta[\mathrm{UFP}]_{\mathrm{peak}})$ ($R^2 = 0.59$). Black dotted line and blue dash-dotted line in plot **(b)** are linear fits for over-pass ($R^2 = 0.63$) and under-pass ($R^2 = 0.67$) freeway transects, respectively.

ACPD
13, 25253–25290, 2013

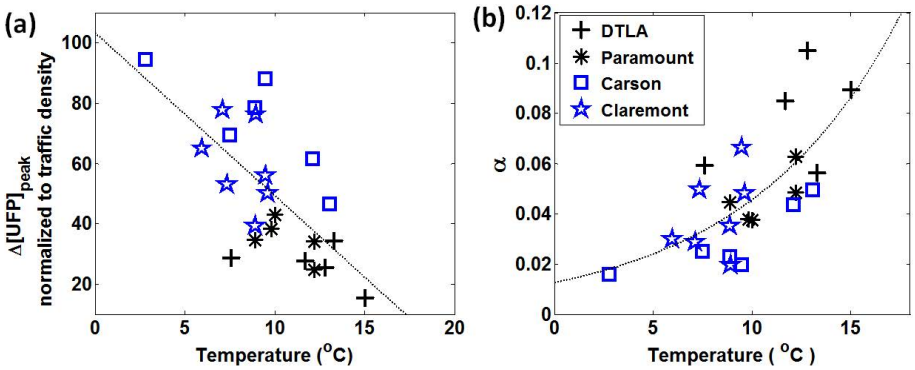

Fig. 7. Temperature effects on **(a)** peak concentration difference from the background ($\Delta[\mathrm{UFP}]_{\mathrm{peak}} = [\mathrm{UFP}]_{\mathrm{peak}} -$ background $[\mathrm{UFP}]_{\mathrm{bkgnd}}$) normalized to traffic density and **(b)** dispersion coefficient α. Black dotted lines are curve fits: **(a)** $\Delta[\mathrm{UFP}]_{\mathrm{peak}} \cdot (\mathrm{Traffic})^{-1} = -5.41 \cdot T + 103.4$ ($R^2 = 0.46$) and **(b)** $\alpha = 1.27 \times 10^{-2} \cdot e^{0.13 \cdot T}$ ($R^2 = 0.48$).

ACPD
13, 25253–25290, 2013

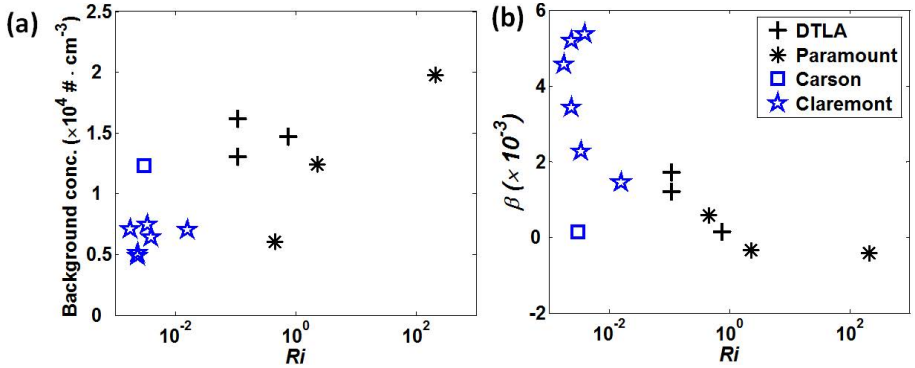

Fig. 8. Dependence of **(a)** background UFP concentrations and **(b)** dispersion coefficient, β on atmospheric stability, represented by the Richardson number (*Ri*).

ACPD
13, 25253–25290, 2013

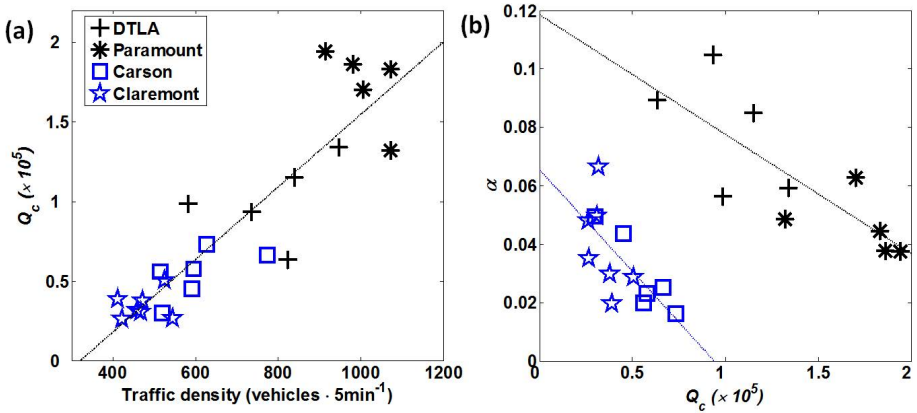

Fig. 9. (a) Emission parameter, Q_c as a function of traffic density (vehicles · 5 min^{-1}) in four sampling sites, and **(b)** α variations as a function of Q_c. Dotted line represents a linear fit to all data points in the plot: **(a)** $Q_c = 227.7 \times$ (Traffic flow) $- 7.3 \times 10^4$ ($R^2 = 0.80$) and **(b)** $\alpha = -4.1 \times 10^{-7} \cdot Q_c + 0.12$ ($R^2 = 0.63$ for overpass freeways) and $\alpha = -6.95 \times 10^{-7} \cdot Q_c + 0.065$ ($R^2 = 0.51$ for underpass freeways).

ACPD
13, 25253–25290, 2013

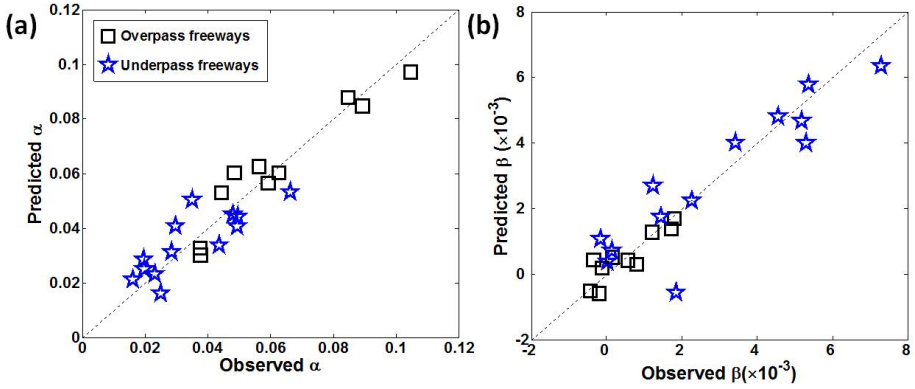

Fig. 10. Comparisons of predicted dispersion coefficients **(a)** α (R^2 = 0.88) and **(b)** β (R^2 = 0.86) with observations. Black squares are for the overpass freeway transects (DTLA and Paramount) and blue stars for underpass freeways (Carson and Claremont). Dotted line represents 1 : 1 relationship.

ACPD
13, 25253–25290, 2013